JMEPEG (2016) 25:2043–2052
DOI: 10.1007/s11665-016-2049-9

1059-9495/$19.00

The Effects of Stress Triaxiality, Temperature and Strain Rate on the Fracture Characteristics of a Nickel-Base Superalloy

Jianjun Wang, Weiguo Guo, Jin Guo, Ziang Wang, and Shengli Lu

(Submitted August 3, 2015; in revised form March 27, 2016; published online April 12, 2016)

In this work, to study the effects of stress triaxiality, temperature, and strain rate on the fracture behaviors of a single-crystal Nickel-base superalloy, a series of experiments over a temperature range of 293 to 1373 K, strain rate range of 0.001 to 4000/s, and stress triaxiality range of −0.6 to 1.1 are conducted. Anomalous peak of stress is noticed in the yield stress versus temperature curves, and strain rate effect on the anomalous peak of yield stress is analyzed. The anomalous peak shifts to higher temperature as the strain rate increases. Then the effects of stress triaxiality, temperature, and strain rate on its fracture behaviors, including strain to fracture, path of crack propagation, and fracture surface, are observed and analyzed. A valley of the fracture strain is formed in the fracture strain versus temperature curve over the selected temperature range. The micrograph of fracture surface is largely dependent on the temperature, stress triaxiality, and strain rate. Finally, the original Johnson-Cook (J-C) fracture criterion cannot describe the effect of stress triaxiality and temperature on the fracture behaviors of single-crystal Nickel-base superalloy. A modified J-C fracture criterion is developed, which takes the anomalous stress triaxiality and temperature effects on the fracture behaviors of single-crystal Nickel-base superalloy into account.

Keywords fracture criterion, single-crystal nickel-base superalloy, strain rate, stress triaxiality, temperature

1. Introduction

The performance of the aircraft engine is highly depending on the properties of its materials, especially the material of turbine blades. The extreme environment within the turbine engine requires superior high-temperature properties in turbine blades. Single-crystal Nickel-base superalloy (SCNBS) has no grain boundary, which causes the brittleness of polycrystals at high temperature (Ref 1, 2). SCNBSs are widely used as turbine blades due to their superior mechanical performances at high temperature (Ref 3).

As studied previously (Ref 4-8), yield stress or critical resolved shear stress (CRSS) increases with increasing temperature over an elevated temperature range and then decreases, e.g., a stress peak occurs. The peak temperature, T_p, and the height of the peak depend on the crystal's orientation, the sense of the applied stress, the deformation rate, and sensitively on the exact composition of the γ'-phase (Ref 9). T_p shifts to a higher temperature with increased strain rate (Ref 4, 10). This phenomenon is similar to the strain rate effect of the third-type strain aging (third SA) (Ref 11-13). For the fracture strain of SCNBSs, with the increasing temperature, a valley of fracture strain is observed in the fracture versus temperature curves (Ref 1, 8, 14).

As we known, stress triaxiality has important significance to the void growth. It has been recognized to control the void growth rate leading to ductile failure (Ref 15, 16). For low stress triaxiality, the fracture of the material is ductile. For high stress triaxiality, the fracture is brittle. To obtain a range of stress triaxiality factor, Bridgman (Ref 17) machined notches of different notch severity in plain and cylindrical tensile specimens, and only positive stress tiaxialities were obtained. Bao and Wierzbicki (Ref 18) performed a series of tests including upsetting tests, shear tests, and tensile tests on 2024-T351 aluminum alloy, which cover a wide range of stress triaxialities.

As observed in NIMONIC 105 by Nembach et al. (Ref 19), under the condition $T < T_p$, the yield strength is independent of the temperature and the strain rate, whereas the value of the yield strength is dependent on the temperature and the strain rate for $T > T_p$. This result is in agreement with that obtained by Milligan and Antolovich (Ref 20). However, all of these results were obtained under quasi-static conditions. As a matter of fact, while in service, the turbine blades have severe operation conditions characterized not only by creep, fatigue, corrosion, and oxidation, but also by foreign object impact (Ref 21), which causes significant reduction in the blade's lifetime. Therefore, investigations on the high strain rate properties of SCNBSs are indispensible.

Various fracture criteria were proposed to predict the onset of fracture in metal based on various hypotheses, experimental observations, and analytical studies for nucleation, growth, and coalescence of voids (Ref 22). Based on the equation about void propagation (Ref 15, 23), Johnson and Cook (Ref 24) have proposed a relation for fracture strain as a function

Jianjun Wang, Weiguo Guo, Jin Guo, and **Shengli Lu**, School of Aeronautics, Northwestern Polytechnical University, Xi'an 710072, China; and **Ziang Wang**, AVIC Aviation Powerplant Research Institute, Zhuzhou 412002, China. Contact e-mails: jianjunw87@126.com and weiguo@nwpu.edu.cn.

of stress triaxiality, strain rate and temperature. The Johnson-Cook (J-C) fracture criterion can be expressed as

$$\begin{aligned}\varepsilon_f &= f_1(\sigma_0^*) f_2(\dot{\varepsilon}) f_3(T) \\ &= \left(C_1 + C_2 \exp\left(C_3 \sigma_0^*\right)\right)(1 + C_4 \ln \dot{\varepsilon}^*)(1 + C_5 T^*),\end{aligned} \quad \text{(Eq 1)}$$

where ε_f is the equivalent plastic strain to fracture, $\sigma_0^* = \frac{\sigma_m}{\bar{\sigma}}$ is the stress triaxiality, σ_m is the mean stress, $\bar{\sigma}$ is the von Mises equivalent stress, $\dot{\varepsilon}^* = \dot{\varepsilon}/\dot{\varepsilon}_0$ is the dimensionless strain rate, $\dot{\varepsilon}_0$ is reference strain rate. To simplify the fitting process, one always selected the lowest strain rate of the experiments as the reference strain rate. $T^* = (T - T_r)/(T_m - T_r)$ is homologous temperature, T_r is reference temperature, T_m is the melting temperature. C_1, C_2, C_3, C_4, C_5 are five material constants. Because necking or notch exists in the specimen for tension tests, the deformation of the smooth or notch specimen is not uniform, and the fracture strain occurs at the fracture surface. Based on the assumption that the strain is constant across the minimum cross-section (i.e., the center of the notch), and that the cross-section shape remains unaltered during the deformation, the strain to fracture, ε_f, is calculated as (Ref 25)

$$\varepsilon_f = \ln\left(\frac{A_0}{A_f}\right) = 2\ln\left(\frac{a_0}{a_f}\right), \quad \text{(Eq 2)}$$

where A_0 is the initial area of the minimum cross-section, A_f is the fracture area of the minimum cross-section, a_0 is the initial radius of the minimum cross-section, and a_f is the fracture radius of the minimum cross-section. Due to the simplicity of formulation, the ease of calibration, and the wide availability of material constants for many metals, J-C fracture criterion has been widely applied to engineering.

In this study, a comprehensive experimental study is designed to investigate the effect of temperature (293 to 1373 K), strain rates (0.001 to 4000/s), and stress triaxialities (−0.6 to 1.1) on the fracture characteristics of a SCNBS. Finally, according to the anomalous fracture behaviors of SCNBS, the J-C fracture criterion was modified, and the parameters of the modified J-C fracture criterion are calibrated.

2. Material and Experimental Procedure

2.1 Material and Specimen

The investigated material is selected to be DD407 SCNBS. It was provided by Central Iron and Steel Research Institute of China. To further improve the performance of turboshaft engine, DD407 superalloy was developed in about 2011. Its chemical composition is listed in Table 1. Tensile strength of DD407 and some other SCNBSs of the same generation is shown in Fig. 1. As seen in this figure, the tensile strength of DD407 is higher than that of other superalloys over most of the selected temperature range. Anomalous peak of stress can be observed for all these superalloys, and the peak temperatures for all these SCNBSs are close to each other.

Table 1 Nominal composition of DD407 superalloy (wt.%)

Ni	Cr	C_o	M_o	W	Al	Ti	Ta
Balance	8	5.5	2.25	5	6	2	3.5

The SCNBS is hardened by coherent ordered fcc Ni_3Al (γ') particles in the disordered fcc γ matrix (Ref 28). Figure 2 shows the microstructure of DD407 superalloy using scanning electron microscope (SEM). As seen in Fig. 2, the microstructure of the SCNBS mainly consists of submicron cubic γ'-precipitates dispersed in the γ-phase matrix. The specimens used in the experiments are from a rod with a diameter of 16 mm. The crystallographic orientations were examined by a rotation x-ray diffraction method on a D/MAX-2400 x-ray diffractometer. The loading direction (longitudinal direction) of the specimens was within 10° deviating from [001] orientation of the crystal lattice. Figure 3 shows the specimens for compression (including plane strain compression, notched round bar compression, and cylinder compression), tension (including smooth round bar tension and notched round bar tension), and pure shear. For plane strain compression and pure shear, the direction of the length of the cross-section is close to [100] orientation.

2.2 Low Strain Rate Experiments

The compression, tension, and shearing tests at nominal strain rate of 0.001/s are conducted using a DNS100 servohydraulic testing machine, over temperature range of 293 to 1373 K. Elevated temperatures are obtained with a radiant-heating furnace, measuring the temperature using a thermocouple arrangement. The temperature was maintained constant during the test with a fluctuation of ±3 °C. The deformation of the specimen is obtained indirectly by subtracting the displacement due to the compliance of the loading frame from the displacement measured by LVDT, which mounted in the testing machine.

2.3 High Strain Rate Experiments

Dynamic compression experiments are performed at strain rates of 1000 and 4000/s over temperature range of 293 to 1273 K, using the NPU's enhanced split Hopkinson pressure bar technique. The enhanced split Hopkinson bar technique was originally developed by Nemat-Nasser et al. (Ref 29). A furnace was used to attain the required uniform temperature in the specimen during the high-temperature tests. Dynamic tension experiments are performed at strain rate of 1000 and 4000/s and temperature of 293 K, using the NPU's split Hopkinson tensile bar. During the experiments, two improved technique are applied, e.g., high-temperature split Hopkinson pressure bar technique (Ref 30) and dynamic recovery technique (Ref 31, 32).

3. Experimental Results and Analysis

3.1 Plastic Behaviors of SCNBS

Uniaxial compression tests were conducted on the DD407 superalloy along the nominal [001] crystal orientation. The true stress-true strain curves were obtained over a wide range of temperatures from 293 to 1273 K and over strain rate ranging from 0.001 to 4000/s. To further the understanding of the temperature effect on the stress, the yield stress vs. temperature relation of DD407 superalloy is plotted for each applied strain rate in Fig. 4. As seen in this figure, anomalous peak of stress occurs at the indicated strain rates. This anomalous peak has been also observed in the stress versus temperature curves of other SCNBSs (Ref 27). The peak temperature, T_p, is about

1055 K for the strain rate of 0.001/s, 1150 K for 1000/s and 1160 K for 4000/s. T_p shifts to higher value as the strain rate increases. Figure 5 shows the variation of T_p as a function of strain rate. The height of the anomalous peak decreases with increasing strain rate. Because of this anomalous behavior, the common models used for the flow stress can not describe the mechanical behavior of SCNBS. Our previous paper developed a constitutive model, which took the anomalous peak of stress into account (Ref 14).

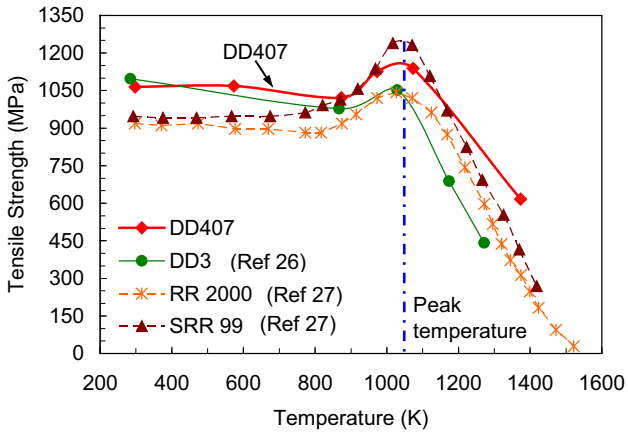

Fig. 1 Quasi-static tensile strength of several SCNBSs as a function of temperature

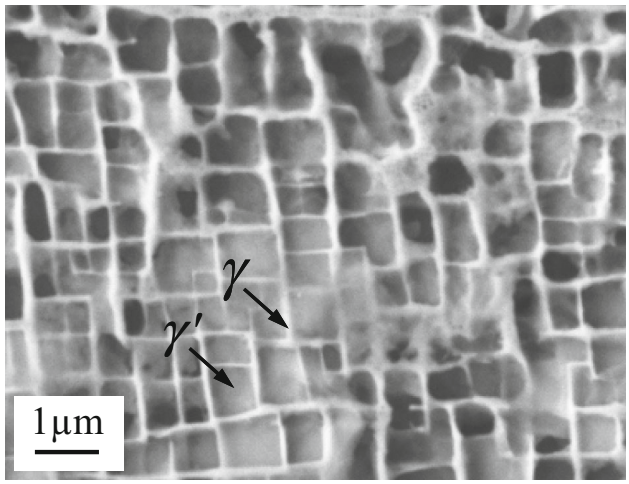

Fig. 2 The SEM micrograph of the DD407 single-crystal superalloy with the scanning surface perpendicular to [001] orientation

3.2 Fracture Behaviors of SCNBS DD407

3.2.1 Effect of Temperature on the Fracture Characteristics. An effort is made in this part to study the effect of temperature on the tensile stress-rupture property of smooth round specimen. Figure 6 shows the variation of the strain to fracture over a temperature range of 293 to 1373 K for DD407 SCNBS. As seen in figure, the strain to fracture first decreases and then increases with the increasing temperature. Thus a valley of the fracture strain is formed over the selected temperature range. The valley temperature of the DD407 superalloy is around 800 K. This anomalous valley of strain to fracture is similar to that of other SCNBS, as shown in Fig. 7. It is obvious that the J-C fracture criterion can not describe such temperature dependence of the strain to fracture.

As seen in the insets of Fig. 6, the path of the crack propagation is temperature dependent. For the case of 293 K,

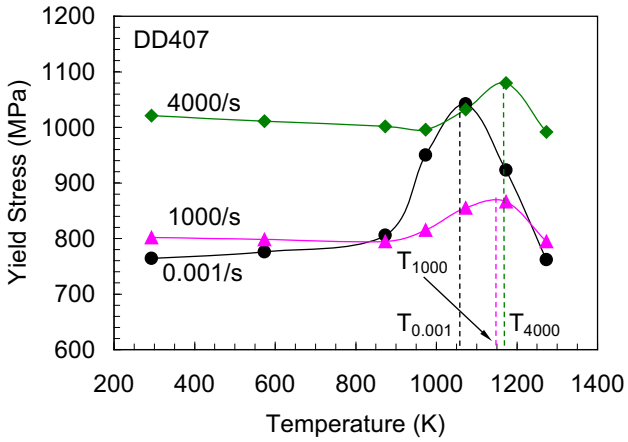

Fig. 4 The yield stress as a function of temperature with indicated strain rates

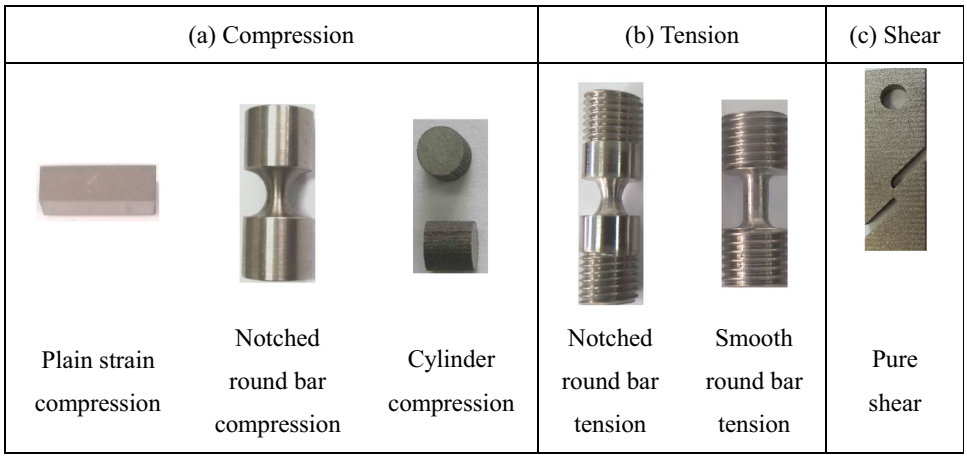

Fig. 3 Specimens types used for tests

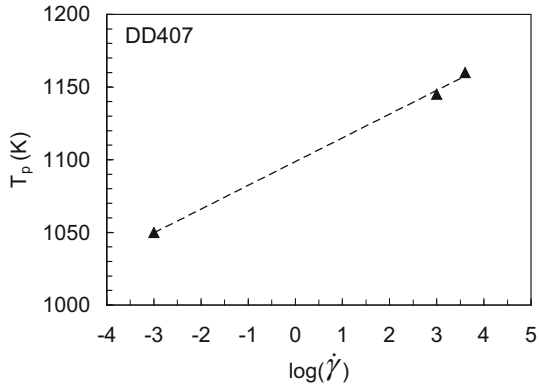

Fig. 5 Viariation of T_p with strain rate

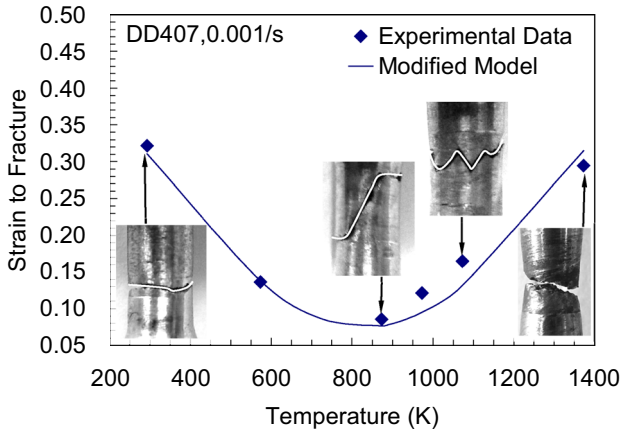

Fig. 6 The temperature-dependent tensile fracturing behaviors of DD407 SCNBS

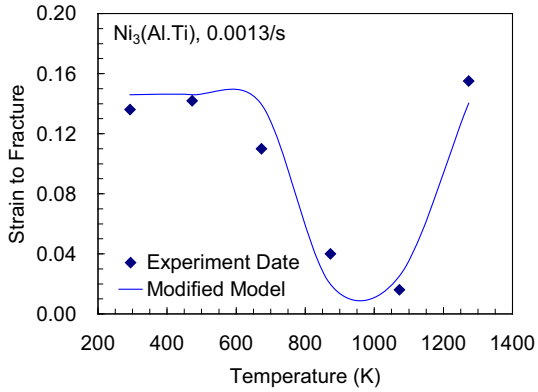

Fig. 7 The temperature-dependent tensile fracturing behaviors of Ni_3(Al·Ti) (from Ref 1)

necking did not occur during the loading process. The crack surface is perpendicular to the loading direction. With the temperature of 873 K, shear fracture is observed. The path of the crack propagation is perpendicular to the loading direction close to the lateral surface of the sample. In the center region of the fractured sample, the crack surface and the loading direction form an angle of about 40°, which is the orientation of the twisted {111} slip plane. With the temperature of 1073 K, the crack surface exhibits a serrated form with an angle of 45° or 135° to the loading direction. The crack propagates alternatively along two groups of octahedral slip planes, which have the same resolved shear stress and strain. In another words, there are two possible paths for crack propagation. Once the crack propagates along one of the slip plane and encounters obstacles, the other path will be taken. For the case of 1373 K, necking is observed close to the fracture surface, which is perpendicular to the loading direction.

Figure 8(a) to (f) shows the SEM micrographs of the tensile fracture surface of DD407 SCNBS with temperature of 293, 873, and 1373 K and strain rate of 0.001/s. For 293 K case, the fracture mode is a mixture of cleavage and microvoid coalescence mechanisms. Microvoids can be observed in the fracture surface. As seen in the inset of Fig. 8(b), the γ' particles are pulled apart because the strength of γ' phase is close to that of γ phase. At 873 K, the fractographs show entire cleavage fracture, and these cleavage planes belong to {111} crystal plane. As seen in the inset of Fig. 8(d), some parts of the edges and corners of the γ'-phase particles are sheared off, and the cracks propagate mainly through the matrix due to the higher strength of γ' phase than that of γ phase at this temperature. At high temperature of 1373 K, the fracture surface is characterized by mostly ductile rupture with dimples. The γ'/γ microstructure can not be observed.

3.2.2 Effect of Stress Triaxiality on the Fracture Characteristics. It is common sense that void growth is mainly affected by the stress triaxiality as analyzed by Mclintck (Ref 23) for a cylindrical void and Rice and Tracey (Ref 15) using a single-spherical void in an infinite solid. Stress triaxiality is an important influence factor of metal ductility, and earlier study results have shown that metal ductility decreases with increasing stress triaxiality (Ref 25, 33). This result is quite natural from the microscope viewpoint of void growth (Ref 22). Bao and Wierzbicki (Ref 18), Bai and Wierzbicki (Ref 34), and Brunig et al. (Ref 35-37) classified damage mechanisms as microshear crack at negative stress triaxiality, void growth-dominated modes at large positive stress triaxiality, and mixed modes for low positive stress triaxiality. To study the effect of stress triaxiality on the plastic strain to fracture of DD407 SCNBS, experiments with different stress triaxialities, including tension, compression, and pure shearing tests, are conducted. Figure 9 shows the geometry of notched specimen. From different geometries of notched specimens, one can obtain different initial stress triaxialities (Ref 24). The initial stress triaxiality σ_0^* in the center of the notch is obtained by inserting the initial radius of the minimum cross-section a_0 and the initial notch radius R_0 into the following Equation (Table 2). In this study, the tensile-notched specimens have initial stress triaxiality equal to 0.56, 0.74, and 1.03 respectively, while the initial minimum radius a_0 equal to 2 mm in all the tensile-notched specimens and the initial notch radius R_0 correspondingly equal to 4, 2, and 1 mm. The test temperature is 1373 K, close to the working temperature of SCNBSs, and the nominal strain rate is 0.001/s.

Figure 10 shows the strain to fracture as a function of stress triaxiality of DD407 SCNBS at temperature of 1373 K and nominal strain rate of 0.001/s and at temperature of 293 K and nominal strain rate of 4000/s. The plastic strain to fracture in pure shear was less than that in uniaxial tension in both of the conditions, which is similar to the Xue's (Ref 38) and Xue and

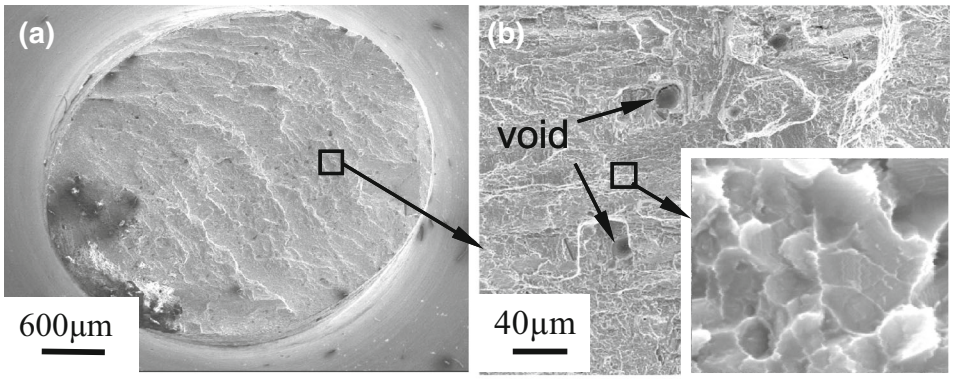

(293 K)

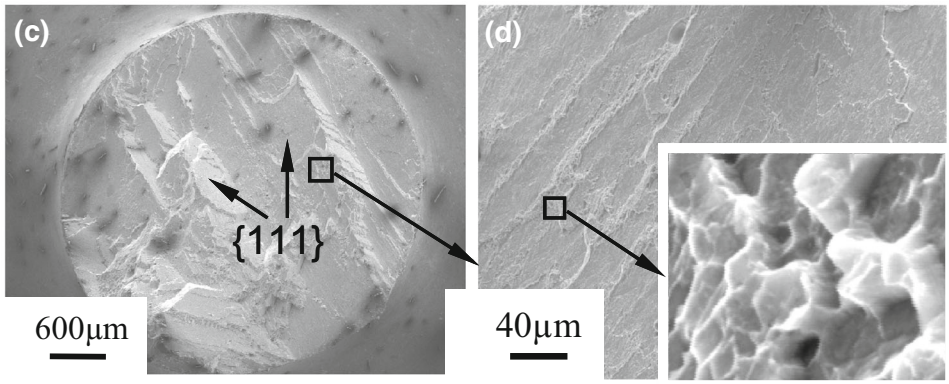

(873 K)

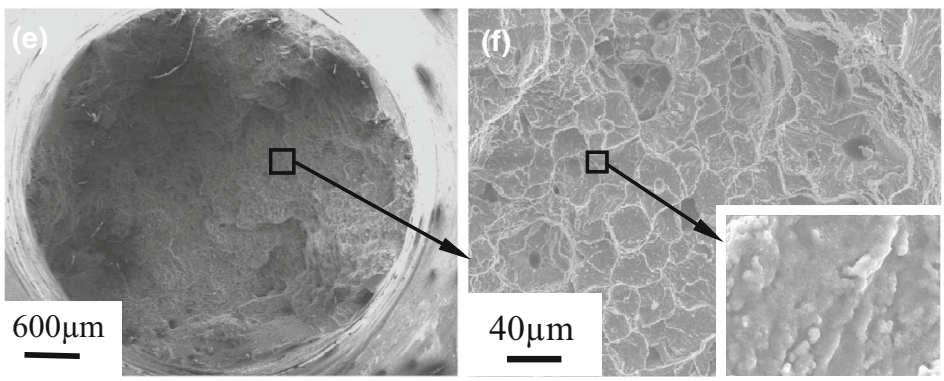

(1373 K)

Fig. 8 The SEM micrographs of the tensile fracture surface of DD407 SCNBS with the temperature of (a, b) 293 K, (c, d) 873 K, (e, f) 1373 K and strain rate of 0.001/s

Wierzbicki's (Ref 39) observation for AA 2024-T351 (Ref 18) and 4340 steel (Ref 40). It is obvious that the J-C fracture criterion can not predict such fracture behavior at both low strain rate and high strain rate, as shown in Fig. 10. With the increasing positive stress triaxiality of tension specimen, the angle of the crack with the loading direction varies from 90° to about 45° at temperature of 1373 K and low strain rate of 0.001/s shown in Fig. 10(a). However, the crack propagation of tension specimen seems insensitive to stress triaxiality at temperature of 293 K and high strain rate of 4000/s, and the crack seems always perpendicular to the loading direction with the varying stress triaxiality, as seen in Fig. 10(b).

The micrographs of fracture surface at temperature of 1373 K, nominal strain rate of 0.001/s, and different stress triaxialities are shown in Fig. 11. For the tension of notched specimen shown in Fig. 11(a) and (b), the fracture surface is characterized by mostly ductile rupture with dimples. Square-shaped facets are observed, and a small micropore can be found in the center of the facet. Combined with fracture surface of smooth specimen tension (Fig. 8f), one can find the quantities

Table 2 The types of classical specimens for different stress triaxialities

Specimen type	Expressions for initial stress triaxiality σ_0^*
Smooth round bars, tension (Fig. 3b)	$\frac{1}{3}$
Notched round bars, tension (Fig. 3b)	$\frac{1}{3}+\ln\left(1+\frac{a_0}{2R_0}\right)$
Shear (Fig. 3c)	0
Cylinders, compression (Fig. 3a)	$-\frac{1}{3}$
Plastic plane strain, compression (Fig. 3a)	$-\frac{\sqrt{3}}{3}$
Notched round bars, compression (Fig. 3a)	$-\left[\frac{1}{3}+\ln\left(1+\frac{a_0}{2R_0}\right)\right]$

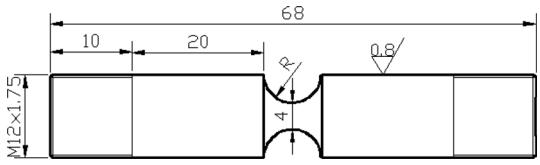

Fig. 9 Geometry and dimensions of notched specimens

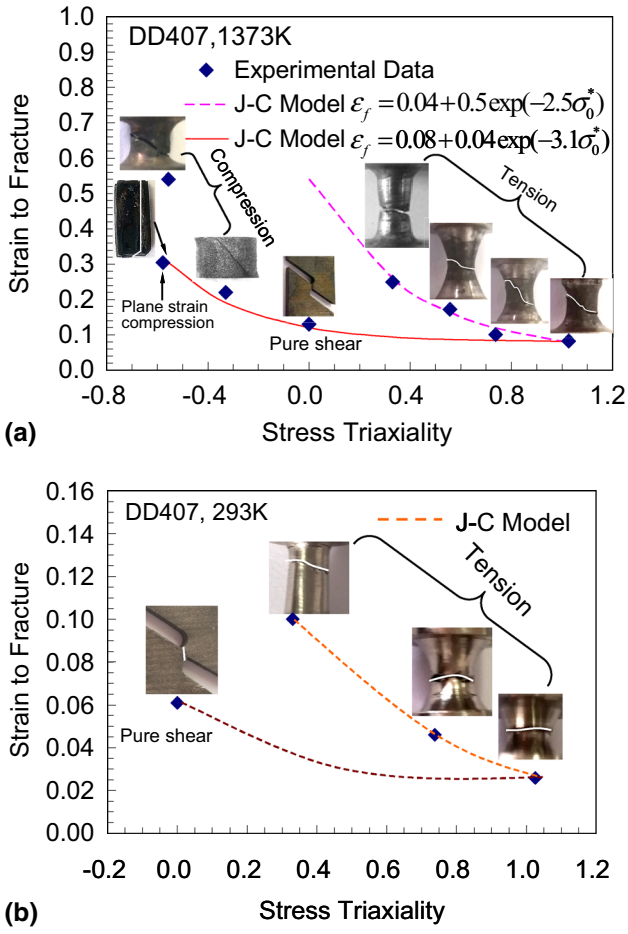

Fig. 10 Strain to fracture as function of stress triaxiality (a) at temperature of 1373 K and nominal strain rate of 0.001/s (b) at temperature of 293 K and nominal strain rate of 4000/s

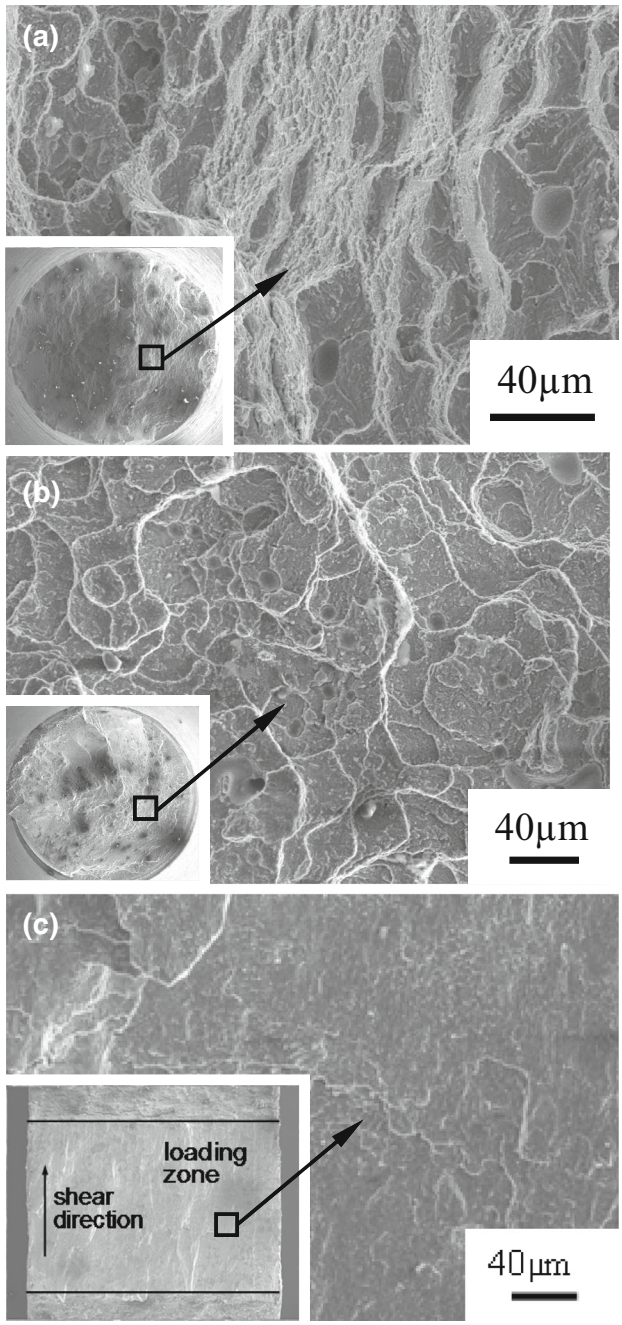

Fig. 11 The SEM micrographs of the fracture surface of DD407 SCNBS with the temperature of 1373 K and strain rate of 0.001/s. (a) Notched tension with = 1.03, (b) notched tension with =0.74, and (c) pure shear

of facets and micropores decrease with the increasing stress triaxiality. For pure shear, fracture mode completely changes to cleavage mechanism, as shown in Fig. 11(c). The micrographs of fracture surface at temperature of 293 K, nominal strain rate of 4000/s, and stress triaxiality of 1.03 are shown in Fig. 12. The characteristics of fracture surface at high strain rate are quite different from that under quasi-static condition. Lots of needle-shaped defects can be seen in the fracture surface, as the arrows point in Fig. 12. Two kinds of fracture morphology are observed, as shown in the enlarged partial view of Fig. 12. One

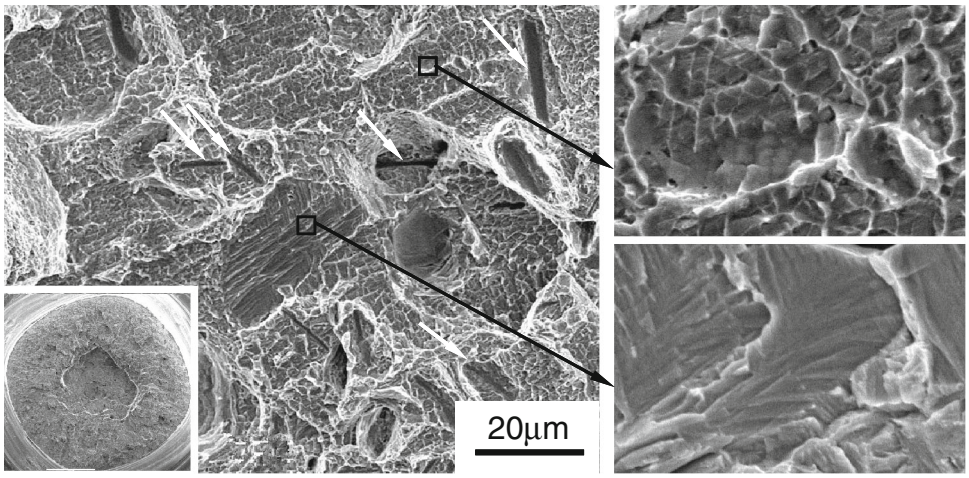

Fig. 12 The SEM micrographs of the fracture surface of DD407 SCNBS with the temperature of 293 K and strain rate of 4000/s for notched tension with =1.03

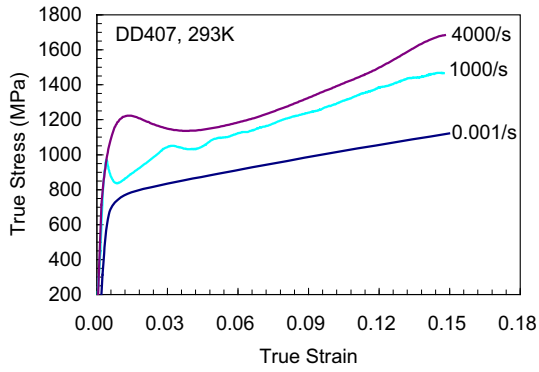

Fig. 13 The true stress-true strain relation of DD407 with temperature of 293 K and strain rate of 0.001, 1000, and 4000/s

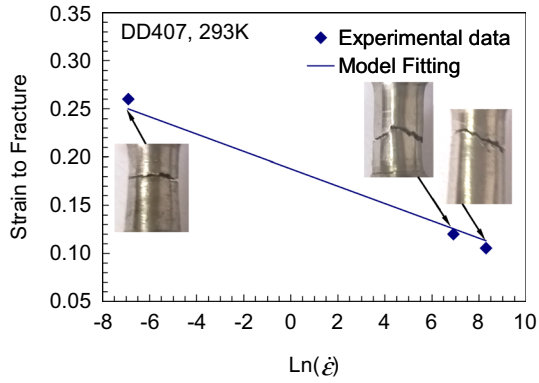

Fig. 14 The comparison of the fitting curve with experimental results

presents the γ/γ' microstructure, and the other shows glacier-like fracture morphology.

3.2.3 Strain Rate Effect on the Fracture Characteristics. Tensile experiments with smooth specimens are conducted at temperature of 293 K and different strain rates (0.001, 1000, and 4000/s), as shown in Fig. 13. The flow stress of DD407 SCNBS is sensitive to strain rate. Figure 14 shows the fracture strain versus strain rate relation. The fracture strain decreases linearly with increasing $\ln(\dot{\varepsilon})$, which can be described by J-C fracture criterion. The crack propagation is dependent on strain rate. At low strain rate of 0.001/s, the crack surface is perpendicular to the loading direction. For high strain rate case (1000 and 4000/s), the crack surface is inclined to loading direction. The micrograph of fracture surface of tension smooth specimen at temperature of 293 K and high strain rate of 4000/s is shown in Fig. 15. Comparing with the fracture surface at temperature of 293 K and low strain rate of 0.001/s (Fig. 8b), lots of needle-shaped defects in the fracture surface at high strain rate, as the arrows point in Fig. 15. Two kinds of fracture morphology, which are similar to that at temperature of 293 K, strain rate of 4000/s, and stress triaxiality of 1.03 (Fig. 12), are observed, as shown in the enlarged partial view of Fig. 15. Similarly, one presents the γ/γ' microstructure, and the other shows glacier-like fracture morphology.

4. Discussion

As discussed in previous section, the J-C fracture criterion can not describe the effects of temperature and stress triaxiality on the fracture behaviors of DD407 SCNBS. For the original expression of J-C fracture criterion, the strain to fracture is given as multiplication of the stress triaxiality, temperature, and strain rate term, $\varepsilon_f = f_1(\sigma_0^*) f_2(\dot{\varepsilon}) f_3(T)$. To exactly describe the effect of stress triaxiality, temperature, and strain rate on the strain to fracture of SCNBSs, a modified J-C fracture criterion should be developed.

As described above, the stress triaxiality term of J-C fracture criterion, $f_1(\sigma_0^*)$, can not describe the stress triaxiality effect on the fracture behavior. A modified J-C fracture criterion should be developed to describe the effect of stress triaxiality on the strain to fracture. As pointed out by Barsoum and Faleskog (Ref 41), based on previous experimental work (Ref 18, 42) and our experimental results, the stress state term of a model incorporating only stress triaxiality cannot predict the fracture characteristics of metals. Previous studies (Ref 38, 39, 43) have shown that Lode parameter, besides stress triaxiality, has

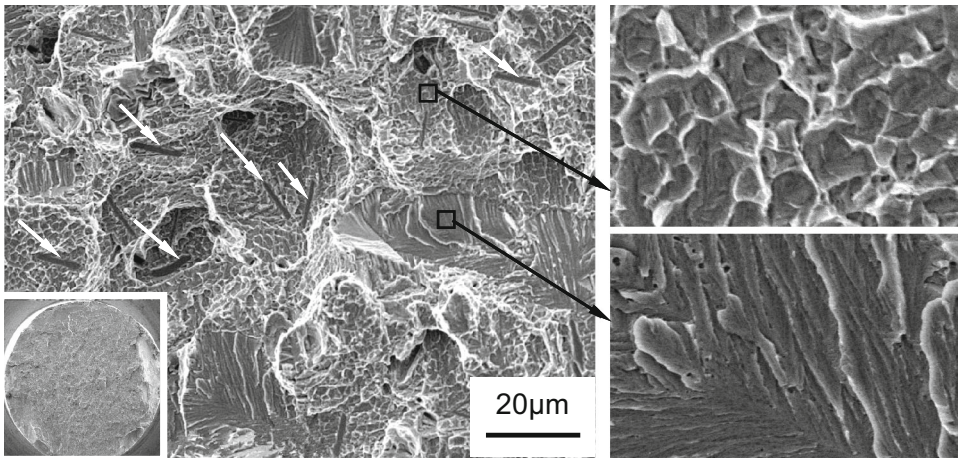

Fig. 15 The SEM micrographs of tensile fracture surface of DD407 SCNBS with the temperature of 293 K and strain rate of 4000/s

important influence on the fracture characteristic. Wilkins et al. (Ref 44) were first to introduce the effect of deviatoric stress ratio, which is related to Lode parameter on ductile fracture, on fracture. Lode parameter dependence was first introduced in modeling of fracture by Xue (Ref 38). Lode parameter, L, is defined as

$$L = \frac{2\sigma_2 - \sigma_1 - \sigma_3}{\sigma_1 - \sigma_3}, \qquad \text{(Eq 3)}$$

where σ_1, σ_2, and σ_3 indicates the largest, middle, and the lowest principle stress respectively, ordered as $\sigma_1 \geq \sigma_2 \geq \sigma_3$. L changes from 1 to −1. As a result of the competition of two failure mechanisms: void growth and "shear decohesion," the fracture locus would exhibit three branches in the whole range of the stress triaxiality (Ref 18, 45). Hence, the following simple form of strain to fracture as a function of stress triaxiality and Lode parameter is postulated (Ref 34),

$$F_1\left(\sigma_0^*, L\right) = \left[\frac{1}{2}\left(D_1 e^{-D_2\sigma_0^*} + D_5 e^{-D_6\sigma_0^*}\right) - D_3 e^{-D_4\sigma_0^*}\right]L^2 + \frac{1}{2}\left(D_1 e^{-D_2\sigma_0^*} - D_5 e^{-D_6\sigma_0^*}\right)L + D_3 e^{-D_4\sigma_0^*}, \qquad \text{(Eq 4)}$$

where D_1, D_2, D_3, D_4, D_5, and D_6 are parameters. For tension, $L = -1$, and value of D_5 and D_6 can be obtained based on the corresponding experimental results. For notched round bar compression and cylinder compression, $L = 1$, and value of D_1 and D_2 can be obtained according to experimental results. Finally, D_3 and D_4 can be calibrated according to the experimental results of pure shear and plane strain compression. Values of these parameters are shown in Table 3. Figure 16(a) shows the comparison of the fracture criterion predictions with the experimental results under quasi-static condition. To further verify the proposed model, Fig. 16(b) compares the fracture criterion predictions with the experimental results at high strain rate (4000/s). As seen in these figure, the model predictions agree well with the experimental results at the selected stress triaxialities, Lode parameters, temperatures, and strain rates.

As discussed in Sect. 3.2.1, the fracture strain first decreases and then increases with the increasing temperature for SCNBS, as shown in Fig. 6 and 7. J-C fracture criterion can not describe such fracture behavior. Based on the experimental data, a

Table 3 Calibrated parameters of modified J-C fracture criterion

D_1	D_2	D_3	D_4	D_5	D_6	D_7	T_0	T_Δ	D_8
0.18	3.6	0.31	1.5	1	1.8	0.9	830	820	−0.036

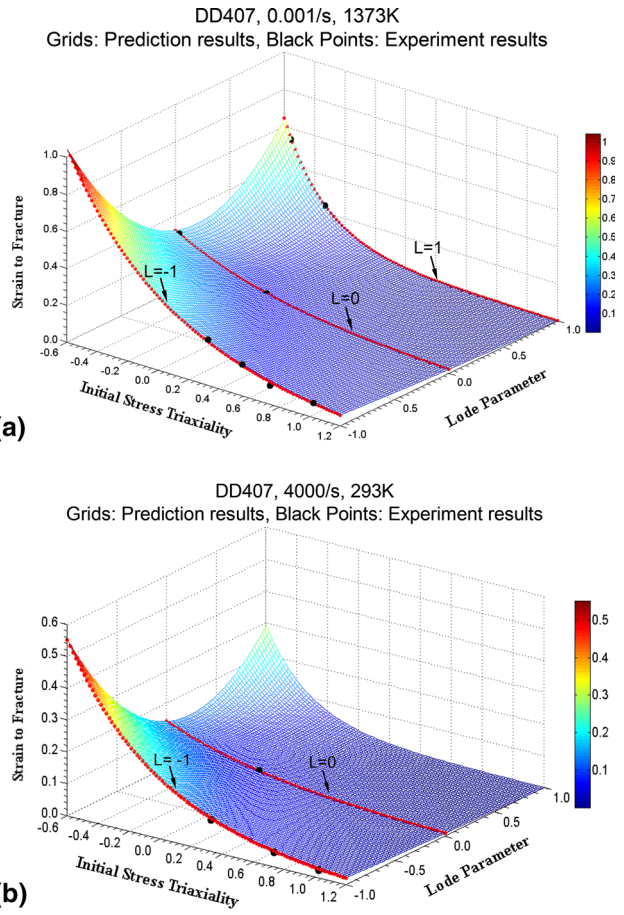

Fig. 16 Comparison of prediction results of the proposed fracture criterion with experimental results (a) at strain rate of 0.001/s and temperature of 1373 K (b) at strain rate of 4000/s and temperature of 293 K

modified form of the temperature term, $F_3(T)$, is developed to describe this anomalous fracture behavior of SCNBSs

$$F_3(T) = 1 - D_7 \exp\left[-\left(\frac{T - T_0}{T_\Delta}\right)^2\right], \quad \text{(Eq 5)}$$

where T_0 is the temperature corresponding to the valley strain to fracture, T_Δ reflects the temperature range of the anomalous valley, D_7 reflects the value of the valley strain to fracture, and T_0, T_Δ, D_7 are all constants.

Generally, the final expression of the modified J-C fracture criterion is given by

$$\varepsilon_f = F_1\left(\sigma_0^*, L\right) F_2(\dot{\varepsilon}) F_3(T), \quad \text{(Eq 6)}$$

where

$$F_1\left(\sigma_0^*, L\right) = \left[\frac{1}{2}\left(D_1 \mathrm{e}^{-D_2\sigma_0^*} + D_5 \mathrm{e}^{-D_6\sigma_0^*}\right) - D_3 \mathrm{e}^{-D_4\sigma_0^*}\right] L^2 + \frac{1}{2}\left(D_1 \mathrm{e}^{-D_2\sigma_0^*} - D_5 \mathrm{e}^{-D_6\sigma_0^*}\right) L + D_3 \mathrm{e}^{-D_4\sigma_0^*}, \quad \text{(Eq 7)}$$

$$F_2(\dot{\varepsilon}) = (1 + D_8 \ln \dot{\varepsilon}^*), \quad \text{(Eq 8)}$$

$$F_3(T) = 1 - D_7 \exp\left[-\left(\frac{T - T_0}{T_\Delta}\right)^2\right]. \quad \text{(Eq 9)}$$

All the model parameters can be calibrated using experimental data, the value of the parameters are shown in Table 3.

5. Conclusion

In this work, a comprehensive experimental investigation on a SCNBS (DD407) is carried out over a temperature range of 293 to 1373 K, strain rate range of 0.001 to 4000/s, and stress triaxiality range of −0.6 to 1.1. The temperature, strain rate, and stress triaxiality effect on the fracture behaviors and strain rate effect on the anomalous yield stress peak are analyzed. Based on the experimental results, a modified J-C fracture criterion is developed, which is shown to work well for describing the fracture behavior of DD407 SCNBS. The following conclusions can be drawn from this study:

1. The anomalous peak of the stress takes place at both low and high strain rates. The peak temperature is about 1055 K for the strain rate of 0.001/s, 1150 K for 1000/s, and 1160 K for 4000/s. The peak of the stress shifts to higher temperature with increased strain rate.
2. A valley of the fracture strain is formed in the fracture strain versus temperature curves over the selected temperature range.
3. The micrograph of fracture surface is largely dependent on the temperature, stress triaxiality, and strain rate.
4. The J-C fracture criterion is modified, and its prediction results agree well with the experimental results at the selected stress triaxialities, Lode parameters, temperatures, and strain rates.

Acknowledgment

This research work was supported by the National Natural Science Foundation of China (Nos. 11372255 and 11572261) and Innovation Foundation for Doctor Dissertation of Northwestern Polytechnical University (No. CX201508).

References

1. K. Aoki and O. Izumi, Flow and Fracture Behaviour of Ni_3(Al·Ti) Single Crystals Tested in Tension, *J. Mater. Sci.*, 1979, **14**, p 1800–1806
2. J.C. Chang, Y.H. Yun, C. Choi, and J.C. Kim, Development of Microstructure and Mechanical Properties of Ni-Base Single-Crystal Superalloy by Hot-Isostatic Pressing, *J. Mater. Eng. Perform.*, 2003, **12**, p 420–425
3. T. Khan, and P. Caron, Advanced Superalloys for Turbine Blade and Vane Applications, in *C/M Symposium on "Advance in Gas Turbine Engine Materials"*, vol. 1 (Ottawa, 1991), p 1–17
4. G.R. Leverant, M. Gell, and S.W. Hopkins, The Effect of Strain Rate on the Flow Stress and Dislocation Behavior of a Precipitation-Hardened Nickel-Base Alloy, *Mater. Sci. Eng. A*, 1971, **8**, p 125–133
5. A. Sengupta, S.K. Putatunda, L. Bartosiewicz et al., Tensile Behavior of a New Single-Crystal Nickel-Based Superalloy (CMSX-4) at Room and Elevated Temperatures, *J. Mater. Eng. Perform.*, 1994, **3**, p 73–81
6. E. Nembach, The High Temperature Peak of the Yield Strength of γ'-Strengthened Superalloys, *Mater. Sci. Eng. A*, 2006, **429**, p 277–286
7. L.N. Wang, Y. Liu et al., Orientation and Temperature Dependence of Yielding and Deformation Behavior of a Nickel-Base Single Crystal Superalloy, *Mater. Sci. Eng. A*, 2009, **505**, p 144–150
8. X.G. Wang, J.L. Liu, T. Jin, and X.F. Sun, Tensile Behaviors and Deformation Mechanism of a Nickel-Base Single Crystal Superalloy at Different Temperature, *Sci. Eng. A*, 2014, **598**, p 154–161
9. D.P. Pope and S.S. Ezz, Mechanical Properties of Ni_3Al and Nickel-Base Alloys with High Volume Fraction of γ', *Int. Met. Rev.*, 1984, **29**, p 136–167
10. M.L. Weaver, R.D. Noebe, and M.J. Kaufman, The Influence of C and Si on the Flow Behavior of NiAl Single Crystals, *Scr. Mater.*, 1996, **34**(6), p 941–948
11. W.G. Guo and X. Gao, On the Constitutive Modeling of a Structural Steel Over a Range of Strain Rates and Temperatures, *Mater. Sci. Eng. A*, 2013, **561**, p 468–476
12. J. Su, W.G. Guo, W.H. Meng, and J.J. Wang, Plastic Behavior and Constitutive Relations of DH-36 Steel Over a Wide Spectrum of Strain Rates and Temperatures Under Tension, *Mech. Mater.*, 2013, **2013**(65), p 76–87
13. J.J. Wang, W.G. Guo, X. Gao, and J. Su, The Third-Type of Strain Aging and the Constitutive Modeling of a Q235B Steel Over a Wide Range of Temperatures and Strain Rates, *Int. J. Plast.*, 2015, **65**, p 85–107
14. J.J. Wang, W.G. Guo et al., Anomalous Behaviors of a Single-Crystal Nickel-Base Superalloy Over a Wide Range of Temperatures and Strain Rates, *Mech. Mater.*, 2016, **94**, p 79–90
15. J.R. Rice and D.M. Tracey, On the Ductile Enlargement of Voids in Triaxial Stress Fields, *J. Mech. Phys. Solids*, 1969, **17**, p 201–217
16. M.S. Mirza and D.C. Barton, The Effect of Stress Triaxiality and Strain-Rate on the Fracture Characteristics of Ductile Metals, *J. Mater. Sci.*, 1996, **31**, p 453–461
17. P.W. Bridgman, *Studies in Large Plastic Flow and Fracture with Special Emphasis on the Effects of Hydrostatic Pressure*, McGraw-Hill, New York, 1952
18. Y. Bao and T. Wierzbicki, On Fracture Locus in the Equivalent Strain and Stress Triaxiality Space, *Int. J. Mech. Sci.*, 2004, **46**, p 81–98
19. E. Nembach, J. Pesicka, and E. Langmaack, The High-Temperature Decrease of the Yield Strength of the γ'-Strengthened Superalloys NIMONIC PE16 and NIMOMIC 105, *Mater. Sci. Eng. A*, 2003, **362**, p 264–273
20. W.W. Milligan and S.D. Antolovich, Yielding and Deformation Behavior of the Single Crystal Superalloy PWA 1480, *Metall. Trans. A*, 1987, **18A**, p 85–95
21. Z. Mazur, A. Luna-Ramirez, J.A. Juarez-Islas, and A. Campos-Amezcua, Failure Analysis of a Gas Turbine Blade made of Inconel 738LC Alloy, *Eng. Fail. Anal.*, 2005, **12**, p 474–486
22. Y.S. Lou and H. Huh, Evaluation of Ductile Fracture Criteria in a General Three-Dimensional Stress State Considering the Stress Triax-

iality and the Lode Parameter, *Acta Mech. Solida Sin.*, 2013, **26**, p 642–658
23. F.A. McClintock, A Criterion for Ductile Fracture by the Growth of Holes, *Trans. ASME J. Appl. Mech.*, 1968, **35**(3), p 363–371
24. J.W. Johnson and W.H. Cook, Fracture Characteristics of Three Metals Subjected to Various Strains, Strain Rates, Temperatures and Pressures, *Eng. Fract. Mech.*, 1985, **21**, p 31–48
25. J.W. Hancock and A.C. Mackenzie, On the Mechanisms of Ductile Failure in High-Strength Steels Subjected to Multi-Axial Stress-States, *J. Mech. Phys. Solids*, 1976, **24**, p 147–169
26. Z.P. Luo, Z.T. Wu, and D.J. Miller, The Dislocation Microstructure of a Nickel-Base Single-Crystal Superalloy After Tensile Fracture, *Mater. Sci. Eng. A*, 2003, **354**, p 358–368
27. D.W. MacLachlan and D.M. Knowles, Modelling and Prediction of the Stress Rupture Behaviour of Single Crystal Superalloys, *Mater. Sci. Eng. A*, 2001, **302**, p 275–285
28. M.S. Huang, L.G. Zhao, and J. Tong, Discrete Dislocation Dynamics Modeling of Mechanical Deformation of Nickel-Based Single Crystal Superalloys, *Int. J. Plast.*, 2012, **28**, p 141–158
29. S. Nemat-Nasser and J.B. Isaacs, Direct Measurement of Isothermal Flow Stress of Metals at Elevated Temperatures and High Strain Rates with Application to Ta and Ta-W Alloy, *Acta Mater.*, 1997, **45**, p 907–919
30. Y.L. Li, Y.Z. Guo et al., A Critical Assessment of High-Temperature Dynamic Mechanical Testing of Metals, *Int. J. Impact Eng.*, 2009, **36**, p 177–184
31. S. Nemat-Nasser, Y.F. Li, J.B. Isaacs, and J.E. Starrett, Hopkinson Technique for Dynamic Recovery Experiments, *Proc. R. Soc. Lond. Ser. A Math. Phys. Sci.*, 1991, **435**, p 371–391
32. S. Nemat-Nasser, Y.F. Li, and J.B. Isaacs, Experimental/Computational Evaluation of Flow Stress at High Strain Rates with Application to Adiabatic Shear Banding, *Mech. Mater.*, 1994, **17**, p 111–134
33. A.C. Mackenzie, J.W. Hancock, and D.K. Brown, On the Influence of State of Stress on Ductile Failure Initiation in High Strength Steels, *Eng. Fract. Mech.*, 1977, **9**(1), p 167–188
34. Y. Bai and T. Wierzbicki, A New Model of Metal Plasticity and Fracture with Pressure and Lode Dependence, *Int. J. Plast.*, 2008, **24**, p 1071–1096
35. M. Brünig, O. Chyra, D. Albrecht, L. Driemeier, and M. Alves, A Ductile Fracture Criterion at Various Stress Triaxiality, *Int. J. Plast.*, 2008, **24**, p 1731–1755
36. M. Brünig, D. Albrecht, and S. Gerke, Numerical Analyses of Stress-Triaxiality-Dependent Inelastic Deformation Behavior of Aluminum Alloys, *Int. J. Damage Mech.*, 2011, **20**, p 299–317
37. M. Brünig, D. Albrecht, and S. Gerke, Modeling of Ductile Damage and Fracture Behavior Based on Different Micromechanisms, *Int. J. Damage Mech.*, 2011, **20**, p 558–577
38. L. Xue, Damage Accumulation and Fracture Initiation in Uncracked Ductile Solids Subject to Triaxial Loading, *Int. J. Solids Struct.*, 2007, **44**, p 5163–5181
39. L. Xue and T. Wierzbicki, Ductile Fracture Initiation and Propagation Modeling Using Damage Plasticity Theory, *Eng. Fract. Mech.*, 2008, **75**, p 3276–3293
40. G.R. Halford and J. Morrow, On Low-Cycle Fatigue in Torsion, *Proc ASTM*, 1962, **62**, p 695–707
41. I. Barsoum and J. Faleskog, Rupture Mechanism in Combined Tension and Shear, *Int. J. Solids Struct.*, 2007, **44**, p 1768–1786
42. T. Wierzbicki, Y. Bao, Y.W. Lee, and Y. Bai, Calibration and Evaluation of Seven Fracture Models, *Int. J. Mech. Sci.*, 2005, **47**, p 719–743
43. L. Xue and T. Wierzbicki, Numerical Simulation of Fracture Mode Transition in Ductile Plates, *Int. J. Solids Struct.*, 2009, **46**(6), p 1423–1435
44. M.L. Wilkins, R.D. Streit, and J.E. Reaugh, *Cumulative-Strain-Damage Model of Ductile Fracture: Simulation and Prediction of Engineering Fracture Tests, UCRL-53058*. Technical report, Lawrence Livermore Laboratory, Livermore, 1980
45. X. Teng and T. Wierzbicki, Evaluation of Six Fracture Modes in High Velocity Perforation, *Eng. Fract. Mech.*, 2006, **73**, p 1653–1678